Available online at www.sciencedirect.com
SCIENCE DIRECT®
Journal of Solid State Chemistry 170 (2003) 255–264
JOURNAL OF SOLID STATE CHEMISTRY
http://elsevier.com/locate/jssc

Magnetic structure and properties of $Cu_3(OH)_4SO_4$ made of triple chains of spins $s=1/2$

S. Vilminot,[a,*] M. Richard-Plouet,[a] G. André,[b] D. Swierczynski,[a] M. Guillot,[a] F. Bourée-Vigneron,[b] and M. Drillon[a]

[a] *Groupe des Matériaux Inorganiques, IPCMS, UMR 7504 CNRS-ULP, 23 rue du Loess, 67037 Strasbourg Cedex, France*
[b] *Laboratoire Léon Brillouin, CEA-CNRS, CEA-Saclay, 91191 Gif-sur-Yvette Cedex, France*

Received 18 June 2002; received in revised form 12 September 2002; accepted 17 September 2002

Abstract

$Cu_3(OH)_4SO_4$, obtained by hydrothermal synthesis from copper sulfate and soda in aqueous medium, is isostructural with the corresponding antlerite mineral, orthorhombic, space group *Pnma* (62), with $a=8.289(1)$ $b=6.079(1)$ and $c=12.057(1)$ Å, $V=607.5(2)$ Å^3, $Z=4$. Its crystalline structure has been refined from X-ray single crystal and powder neutron diffraction data at room temperature. It consists of copper (II) triple chains, running in the *b*-axis direction and connected to each other by sulfate groups. The magnetic structure, solved from powder neutron diffraction data at 1.4 K below the transition at 5 K evidenced by susceptibility and specific measurements, reveals that, inside a triple chain, the magnetic moments of the copper ions ($\mu_B=0.88(5)$ at 1.4 K) belonging to outer chains are oriented along the *c*-axis of the nuclear cell, with ferromagnetic order inside a chain and antiferromagnetic order between the two outer chains. No long-range magnetic order is obtained along the central chain with an idle spin behavior.

Keywords: Antlerite; Copper hydroxysulfate; Powder neutron diffraction; Magnetic structure; Low-dimensional magnetism; Idle spin

1. Introduction

Hydrothermal synthesis is presently used in our group in Strasbourg to prepare transition metal (Ni, Co, Fe) silicates with clay structure such as 1:1 and 2:1 phyllosilicates of transition metals. These compounds exhibit a ferromagnetic behavior at low temperature [1,2]. Starting from aminopropyltriethoxysilane instead of tetraethoxysilane, a family of hybrid organic–inorganic materials has been isolated and their spectroscopic, thermal, optical and magnetic properties are under study [3]. In the course of this study, attempts to prepare copper phyllosilicates always failed as far as, like for the other transition metals, the corresponding acetate was used. Starting from copper sulfate, small amount of green single crystals was evidenced as copper hydroxysulfate, $Cu_3(OH)_4SO_4$, corresponding to the antlerite mineral. If structural data were already reported for this compound, they were mainly obtained for natural samples and nothing was known about the magnetic properties, stimulating a more complete study of synthetic antlerite. Let us note that the presence of triple chains of copper (II) (spin-1/2), whose interest is currently under scope since they may show in some specific cases an energy gap in the spin excitation spectrum [4], made such a system very exciting from a magnetic point of view.

2. Experimental

2.1. Synthesis

Antlerite has been prepared by hydrothermal treatment of an aqueous suspension obtained from copper sulfate pentahydrate, $CuSO_4.5H_2O$ and soda, NaOH in molar proportions $Cu/Na/H_2O=1/1.333/2222$. The reaction was performed under autogenous pressure in bombs of 125 cm^3, with a ca. 1/3 filling ratio. The precursor suspension was stirred for 1 h before sealing in the reactor that was heated at 170°C for 6 days. At the

*Corresponding author. Fax: +33-3-88-10-72-47.
E-mail address: vilminot@ipcms.u-strasbg.fr (S. Vilminot).

0022-4596/03/$ - see front matter © 2002 Elsevier Science (USA). All rights reserved.
PII: S0022-4596(02)00081-6

end of the reaction, antlerite was obtained in the form of needle-like green single crystals. Attempts to promote crystal growth by introducing seeds in the suspension before hydrothermal treatment were unsuccessful.

For neutron powder diffraction measurements, the same synthesis was used starting from copper sulfate pentahydrate, $CuSO_4\ 5H_2O$, NaOD solution and heavy water D_2O in order to substitute deuterium for hydrogen that exhibits a high incoherent diffusion factor resulting in an increase of the background. Using the same thermal treatment, a powder was obtained instead of single crystals. The powder was filtered and acetone washed. Such washing induces the formation of a small amount of Na_2SO_4.

2.2. Characterization

Thermal analysis was performed with a TG-DTA92 Setaram apparatus, at a 3.5°C/min heating rate, under air. Infrared spectra were recorded on a ATI Mattson spectrometer using the KBr pellet technique.

X-ray powder diffraction patterns were recorded by means of a D5000 Siemens diffractometer ($CuK\alpha_1$, 1.5406 Å). For single-crystal data collection, a single set of 180 frames, 20 s/frame, ϕ scan of 1°/frame (each frame measured twice), crystal detector distance = 30 mm, $\theta = 0°$, $\kappa = 0°$ was collected on a Nonius Kappa CCD diffractometer at the Service Commun de Rayons X, Université Louis Pasteur, Strasbourg. Structure refinement was done starting from the results of Hawthorne et al. [5] using SHELXS-86.

The neutron diffraction experiments were performed at the Laboratoire Léon Brillouin (CEA Saclay) using the 3T2 and G4.1 diffractometers. The high-resolution powder diffractometer 3T2 ($\lambda = 1.2252$ Å, $6° < 2\theta < 126°$) was used for the refinement of the nuclear structure at 300 K and the multi-detector (800 cells) G4.1 ($\lambda = 2.4266$ Å) for the determination of the magnetic structure and the thermal evolution study of the low-temperature patterns. Therefore, 11 diffraction patterns were recorded in the 2θ range 10°–89.9°, at different temperatures between 1.4 and 6 K. The powder sample was set in a cylindrical vanadium can and held in a liquid helium cryostat. Nuclear and magnetic structures were refined using the FULLPROF [6] program. The nuclear scattering lengths ($b_{Cu} = 0.7718 \times 10^{-12}$ cm, $b_S = 0.2847 \times 10^{-12}$ cm, $b_O = 0.5803 \times 10^{-12}$ cm, $b_D = 0.6671 \times 10^{-12}$ cm and $b_H = -0.3739 \times 10^{-12}$ cm) and copper magnetic form factors were those included in this program.

Magnetic susceptibility measurements were performed in the range 2–300 K by means of a Quantum Design MPMS-XL SQUID magnetometer. Specific heat measurements were carried out with a home-made equipment using a quasi-adiabatic method.

3. Results and discussion

3.1. Structural characterization

3.1.1. X-ray powder diffraction

X-ray powder diffraction pattern of the title compound confirms the formation of antlerite, $Cu_3(OH)_4SO_4$, in agreement with JCPDS file 07-407.

3.1.2. Thermal analysis

Thermal analysis reveals a weight loss within two steps (Fig. 1): the first one, between 465°C and 490°C, corresponds to a water loss according to the following reaction:

$$Cu_3(OH)_4SO4 \rightarrow 2CuO + CuSO_4 + 2H_2O$$

the second one, between 730°C and 790°C, corresponds to the decomposition of copper sulfate according to the following reaction:

$$CuSO_4 \rightarrow CuO + SO_3.$$

The observed weight losses do not differ by more than 1% from the calculated ones. X-ray diffraction patterns recorded at different steps of the thermal evolution confirm the above reactions.

3.1.3. Infrared spectroscopy

For deuteriated and hydroxylated compounds, the infrared spectrum (Fig. 2) reveals the presence of four band families, around 3500, 1100, 800 and 600 cm^{-1}. Whereas the intensity and position of the 1100 and 600 cm^{-1} bands are not affected by deuteriation, this is no more the case for the other ones that can be therefore attributed to vibrations involving OH groups. Two sharp bands are observed at around 3573(s) and 3485(s) cm^{-1} and are attributed to OH stretching vibrations. For D partially exchanged sample, they are shifted to 2637(s) and 2576(s) cm^{-1}, respectively. However, the bands related to OH vibrations are still present in relation with a non-complete substitution due to the presence of H_2O coming from copper sulfate pentahydrate. The presence of two bands with similar intensities lead to the conclusion that two kinds of OH groups in equal number are involved. This aspect will be further discussed from neutron diffraction data. Numerous vibrations appear between 880 and 740 cm^{-1}, at 873(m), 852(m), 785(sh) and 754(s) cm^{-1}. Owing to the strong decrease of their intensities after H/D exchange, they are also attributed to vibrations involving OH groups. The ν_3 and ν_4 vibrations of the sulfate group appear as broad and strong bands around 1100 and 600 cm^{-1}, respectively. Due to the distortion from regular tetrahedral symmetry, the degenerate vibrations split into three bands, at 1153(m), 1109(s), 1070(s) cm^{-1} and 634(s), 613(s) and 602(s) cm^{-1} for ν_3 and ν_4, respectively. From point group considerations [7], the

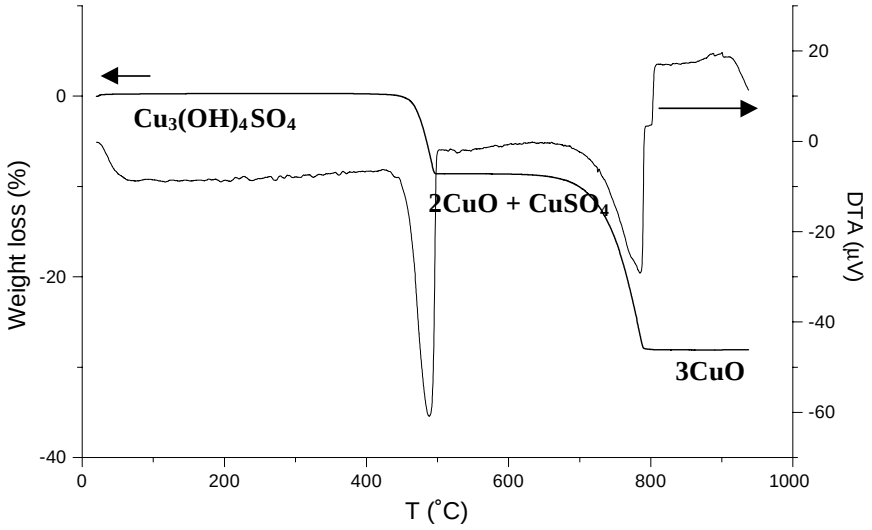

Fig. 1. DTA–TGA traces of antlerite recorded under air with a 3.5°C/min heating rate.

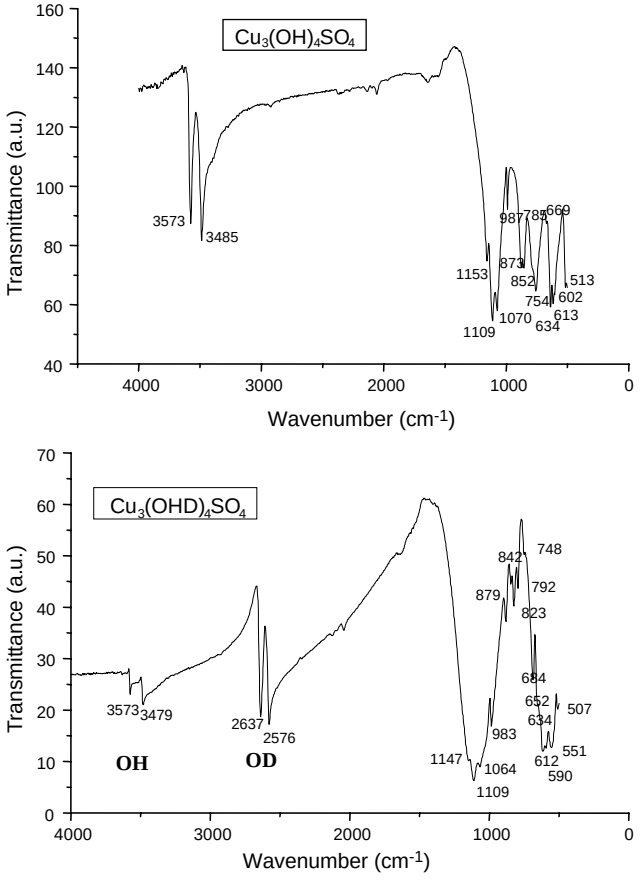

Fig. 2. Infrared spectra of H and D antlerites.

real symmetry is probably C_{2v} for sulfate group. Moreover, a line appears at 987(w) cm^{-1} attributed to ν_1 vibration, normally IR inactive for T_d symmetry but becoming IR active in C_{2v} symmetry. After H/D exchange, any significant shift is not observed and the intensities are of same magnitude. The presence of a new band at around 551(s) cm^{-1} for the D exchanged sample is attributed to a vibration involving OD groups.

3.1.4. *X-ray single-crystal structure*

The structural findings from the single-crystal X-ray diffraction study are very similar to those previously reported for natural antlerite [5]. The lattice parameters, atomic positions, interatomic distances and bond angles are given in Tables 1–3 where OH*i* atoms refer to oxygen atoms of the hydroxyl groups.

The structure may be viewed as a ribbon running along the *b*-axis of three connected chains, each one consisting of edge sharing $Cu(O,OH)_6$ octahedra (Fig. 3). Such chains are connected to each other by SO_4^{2-} anions as depicted in Fig. 4. A similar structure was also evidenced in the case of szenicsite, $Cu_3(OH)_4MoO_4$ [8]. Whereas SO_4 tetrahedra are nearly regular with a mean S–O bond length of 1.481 Å, the octahedra around both crystallographically independent metal ions are strongly distorted, due to the Jahn–Teller distortion usually observed for octahedrally coordinated Copper(II). The equatorial bonds are quite similar (1.977–2.005 Å, 0.7% maximum deviation from the mean value) around Cu1 ions, while the apical bonds differ significantly (2.306–2.552 Å, 5% deviation). The reverse situation is observed for Cu2 where the deviations are stronger (1.925–2.043 Å, 3% deviation) in the equatorial plane compared to the apical direction (2.361–2.428 Å, 1.4% deviation). Considering in more detail the triple chains (Fig. 3), differences appear between the Cu–Cu distances. Whereas all Cu1–Cu1 distances are all the same, it is no more the case for Cu2–Cu2 ones which show alternating distances (3.00 and 3.07 Å) along the *b*-axis. This is related to the fact that SO_4 ions share corners with oxygen belonging to octahedra involving 3.00 Å Cu–Cu distances. On the other hand, copper–copper distances between chains are

larger (3.18 and 3.27 Å). For more details on the structure description, see Ref. [5].

3.1.5. Neutron powder diffraction at room temperature

The results of the structure refinement from neutron powder diffraction measurements at 300 K are summarized in Tables 4 and 5. They allow to evidence a high D content in the sample, around 94%. The O–D bond lengths (Table 3) do not significantly differ from each other with a mean value of 0.960 Å. In all cases, the next-nearest oxygen atom is O3, but the D···O3 distances are quite long, 2.473, 2.481 and 2.183 Å for D1, D2 and D3, respectively. Therefore, it seems that no hydrogen bonding is involved in the case of antlerite. If it was the case, one would expect a more important distortion of the SO_4 tetrahedron, in particular with a much longer S–O3 bond length. However, the differences between the D···O3 distances can explain the infrared results, with two kinds of OH groups in equal number. The observed and calculated diffraction patterns are shown in Fig. 5.

Copper octahedra are connected to each other giving rise to ribbons running in the *b*-axis direction. Such disposition of copper ions appears to be in between one-dimensional (1D) and two-dimensional (2D) systems. Therefore, unusual magnetic properties could be expected in relation with the change of dimensionality.

Table 1
CCD X-ray data collection and structure refinement of synthetic antlerite

a (Å)	8.289(1)	Crystal size (mm^3)	$0.10 \times 0.15 \times 0.22$
b (Å)	6.079(1)	Total reflexions	2870
c (Å)	12.057(1)	Unique reflections	962
V(Å^3)	607.5(2)	Unique $\lvert I_o\rvert > 3\sigma(I_o)$	919
Space group	*Pnma*	R_{int}	0.0362
F(000)	660	R	0.0335
$D_{calc.}$ (g/cm^3)	3.877	wR	0.0446
μ (mm^{-1})	10.73	Goodness-of-fit	1.05
Z	4		

$R = \sum(|F_o| - |F_c|)/\sum|F_o|$,
$wR\left[\sum w(|F_o| - |F_c|)^2\right]/w = 1/(\sigma^2(F) + 0.0032F^2)$.

3.2. Magnetic properties

3.2.1. Magnetic susceptibility

Magnetic susceptibility of the title compound recorded at $H = 100$ Oe follows above 40 K a Curie-Weiss law $\chi = C/(T-\theta) = 1.28/(T-1.69)$ emu/mol^{-1} (Fig. 6), where $C = Ng^2\mu_B^2 S(S+1)/3k$ is the Curie constant, assuming a spin only value with $S = \frac{1}{2}$ for copper(II). The positive θ value is characteristic of a ferromagnetic behavior in the high-temperature regime. From the Curie–Weiss expression, we can deduce a g value of 2.13 as expected. The slight increase of the χT product from room temperature down to 40 K (Fig. 7) confirms the presence of ferromagnetic correlations while the maximum of χ at 6.5 K together with the low temperature χT variation agrees with the presence of competing antiferromagnetic interactions. Finally, at very low temperature, a small downturn of χ is observed at $T = 5$ K (inset of Fig. 6) which points to a transition towards a three-dimensional (3D) long-range order. Such a manifestation is quite unusual in antiferromagic systems at the 1D/3D transition, and so specific heat measurements have been performed to confirm that result.

3.3.2. Specific heat

The temperature dependence of the specific heat, illustrated in Fig. 8, shows a characteristic λ-type anomaly at $T = 5.3$ K, indicating a phase transition towards a 3D state. After deducing the phonon contribution, namely a T^3 contribution in the low-temperature range, and taking into account a T^{-2} tail

Table 2
Final atomic parameters for synthetic antlerite from X-ray data

	x/a	y/b	z/c	U_{iso}[a]	U_{11}[a]	U_{22}[a]	U_{33}[a]	U_{12}[a]	U_{13}[a]	U_{23}[a]
Cu1	0.00472(4)	0.25	0.00129(3)	93(2)	131(3)	100(4)	101(3)	0	−34(2)	0
Cu2	0.28997(4)	0.00288(4)	0.12592(3)	95(2)	109(3)	111(3)	115(3)	−3(1)	−22(1)	12(1)
S	0.13039(8)	0.25	0.36422(6)	78(3)	91(4)	119(4)	74(4)	0	−2(3)	0
O1	0.2616(3)	0.25	0.2829(2)	124(11)	127(11)	210(13)	147(12)	0	39(9)	0
O2	0.1984(4)	0.25	0.4775(2)	147(11)	234(14)	217(13)	99(11)	0	−61(10)	0
O3	0.0313(2)	0.0480(3)	0.3483(2)	131(7)	127(9)	151(8)	198(10)	−28(7)	22(7)	−21(8)
OH1	0.2807(3)	0.25	0.0250(2)	96(10)	159(12)	137(11)	96(11)	0	−6(9)	0
OH2	0.7012(3)	0.25	0.7782(2)	110(10)	165(12)	132(11)	91(11)	0	19(9)	0
OH3	0.0464(3)	0.5067(2)	0.1017(2)	98(7)	118(10)	154(11)	85(10)	−10(5)	9(8)	3(5)
H1	0.362(6)	0.25	0.978(5)	713(197)						
H2	0.274[b]	0.25	0.768[b]	1700[b]						
H3	0.512(11)	0.032(15)	0.664(10)	1712(320)						

OH*i* atoms refer to oxygen atoms of the hydroxyl groups.
[a] $U_{ij} = U_{ij} \times 10^4$ (Å^2), U_{iso} (Å^2) refers to results of the isotropic refinement.
[b] Fixed during refinement.

Table 3
Interatomic distances (Å) and angles (°) for X-ray refinement (upper part) and involving D atoms from powder neutron diffraction data at 300 K (lower part)

S–O1	1.464(3)	O1–S–O2	109.6(3)	⟨O–S–O⟩	109.5
S–O2	1.478(3)	O1–S–O3	108.9(3) × 2		
S–O3	1.490(2) × 2	O2–S–O3	109.2(3) × 2		
S–⟨O⟩	1.481	O3–S–O3	111.0(2)		
Cu1–OH3	1.977(2) × 2	OH3–Cu1–OH3	96.8(1)	OH3–Cu1–OH1	75.8(1) × 2
Cu1–OH3	2.005(2) × 2	OH3–Cu1–OH3	102.2(1)	OH3–Cu1–O2	81.4(2) × 2
Cu1–OH1	2.306(3)	OH3–Cu1–OH3	80.4(1) × 2	OH3–Cu1–O2	96.4(2) × 2
Cu1–O2	2.552(3)	OH3–Cu1–OH3	177(4) × 2	OH1–Cu1–O2	167(1)
⟨Cu1–O⟩	2.137	OH3–Cu1–OH1	106.9(2) × 2		
Cu2–OH2	1.925(2)	OH2–Cu2–OH1	178(5)	OH1–Cu2–O2	91.76(8)
Cu2–OH1	1.935(2)	OH2–Cu2–OH3	95.8(2)	OH1–Cu2–O1	90.3(2)
Cu2–OH3	2.041(3)	OH2–Cu2–O3	88.8(1)	OH3–Cu2–O3	174(2)
Cu2–O3	2.043(2)	OH2–Cu2–O2	86.2(1)	OH3–Cu2–O2	85.0(1)
Cu2–O2	2.361(2)	OH2–Cu2–O1	91.69(9)	OH3–Cu2–O1	91.9(1)
Cu2–O1	2.428(2)	OH1–Cu2–OH3	83.9(1)	O3–Cu2–O2	99.4(2)
⟨Cu2–O⟩	2.122	OH1–Cu2–O3	91.8(1)	O3–Cu2–O1	83.9(1)
				O2–Cu2–O1	176(3)
Cu1–Cu1	3.0407(5) × 2	Cu1–OH3–Cu1	99.6(1)	Cu1–OH1–Cu2	96.7(1) × 2
Cu2–Cu2	3.0042(10)	Cu2–O1–Cu2	76.44(6)	Cu1–OH3–Cu2	103.6(1)
Cu2–Cu2	3.0748(10)	Cu2–OH1–Cu2	101.9(1)	Cu1–O2–Cu2	83.31(9)
Cu1–Cu2	3.1790(12) × 2	Cu2–O2–Cu2	81.26(7)	Cu1–OH3–Cu2	108.9(1)
Cu1–Cu2	3.2684(12) × 2	Cu2–OH2–Cu2	106.0(1)		
D1–OD1	0.955(5)	D1⋯O3	2.474(3) × 2	OD1-D1⋯O3	131.4(7)
D2–OD2	0.962(5)	D2⋯O3	2.481(3) × 2	OD2-D2⋯O3	133.4(7)
D3–OD3	0.963(3)	D3⋯O3	2.183(3)	OD3-D3⋯O3	138.8(7)

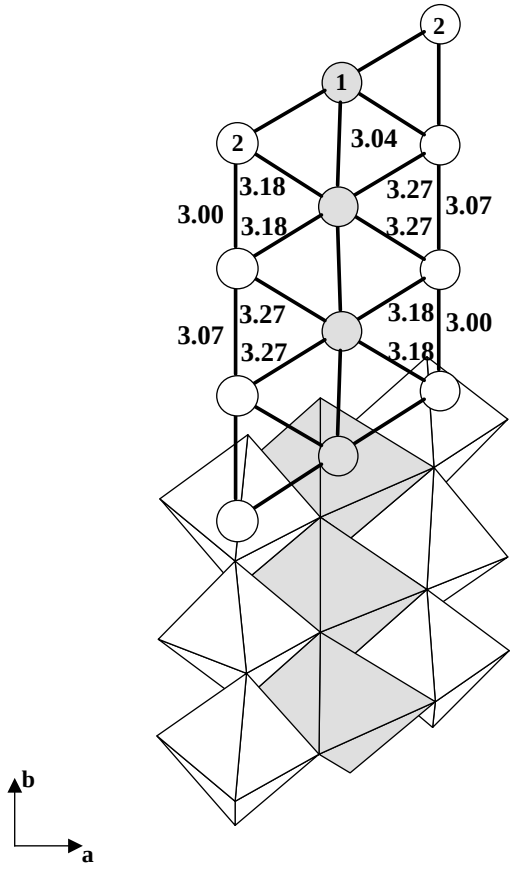

Fig. 3. View of a triple chain of copper octahedra (lower part) running in the *b*-axis direction. Bond lengths inside the triple chain (upper part). Cu1 atoms and octahedra are shaded.

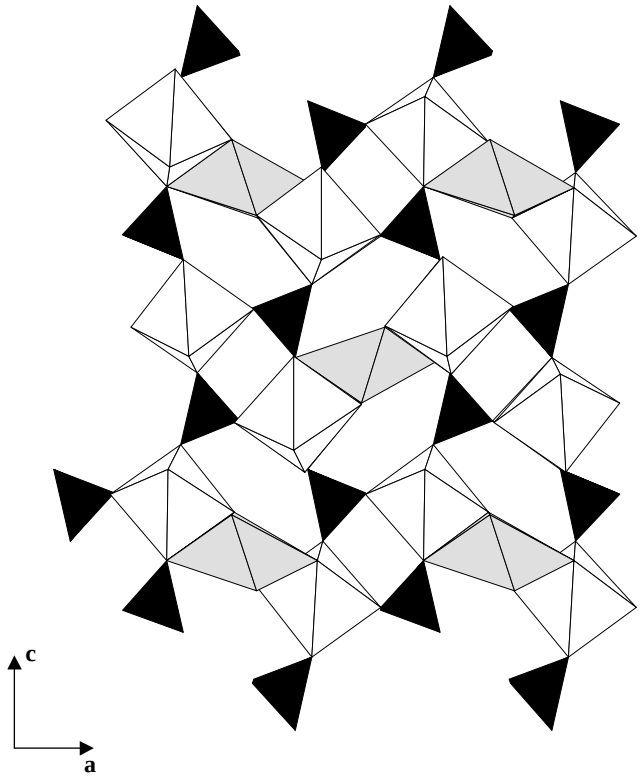

Fig. 4. Projection of the antlerite structure on the *ac* plane.

Table 4
Crystallographic data and refinement characteristics at 300 and 1.4 K from neutron powder data for deuteriated compound

	300 K	1.4 K		300 K	1.4 K
System	Orthorhombic		Number of parameters	58	18
Space group	*Pnma* (62)		R_p (%)	6.72	10.4
a (Å)	8.2574(2)	8.2259(7)	R_{wp} (%)	6.32	11.5
b (Å)	6.0529(1)	6.0466(5)	R_{exp} (%)	4.48	1.59
c (Å)	12.0099(2)	11.9792(10)	R_B (%)	2.87	2.63
Wavelength (Å)	1.2252	2.4266	R_F (%)	1.99	2.28
2θ range and step	6–125.7° 0.05°	10–89.9° 0.1°	Goodness-of-fit (%)	1.99	
Reflections used/total	689/1033	76/247	$R_{magnetic}$(%)		5.04

Table 5
Atomic coordinates and isotropic thermal motion values at 300 K from neutron powder data for deuteriated compound (upper part). Position of the Cu2 magnetic atoms and their magnetic moment from 1.4 K data refinement (lower part)

Atom	*x/a*	*y/b*	*z/c*	Occupancy	*B* (Å2)
Cu1	0.0048(4)	0.25	0.0012(2)	4.0	0.81(3)
Cu2	0.2900(2)	0.0033(3)	0.1262(1)	8.0	0.73(2)
S	0.1307(7)	0.25	0.3635(5)	4.0	0.83(9)
O1	0.2611(4)	0.25	0.2822(3)	4.0	1.08(5)
O2	0.1997(4)	0.25	0.4764(3)	4.0	1.28(5)
O3	0.0316(2)	0.0479(3)	0.3482(2)	8.0	1.07(4)
OH1	0.2808(4)	0.25	0.0248(3)	4.0	0.80(5)
OH2	0.7024(4)	0.25	0.7779(2)	4.0	0.85(5)
OH3	0.0467(2)	0.5062(4)	0.1024(2)	8.0	0.71(3)
H1	0.3633(5)	0.25	0.9696(3)	0.26(2)	2.15(7)
D1	0.3633(5)	0.25	0.9696(3)	3.74(2)	2.15(7)
H2	0.2964(5)	0.25	0.7691(3)	0.31(2)	2.08(6)
D2	0.2964(5)	0.25	0.7691(3)	3.69(2)	2.08(6)
H3	0.5118(3)	0.0125(4)	0.6720(2)	0.38(3)	2.07(4)
D3	0.5118(3)	0.0125(4)	0.6720(2)	7.62(2)	2.07(4)
Atom	*x/a*	*y/b*	*z/c*	$M_x = M_y$	M_z (μ_B)
Cu21	0.2900	0.0033	0.1262	0	−0.88(5)
Cu22	0.2100	−0.0033	0.6262	0	−0.88(5)
Cu23	−0.2900	0.5033	−0.1262	0	0.88(5)
Cu24	0.7900	0.4967	0.3738	0	0.88(5)
Cu25	−0.2900	−0.0033	−0.1262	0	0.88(5)
Cu26	0.7900	0.0033	0.3738	0	0.88(5)
Cu27	0.2900	0.4967	0.1262	0	−0.88(5)
Cu28	0.2100	0.5033	0.6262	0	−0.88(5)

for the magnetic contribution, we deduce the specific heat of magnetic origin (Fig. 8) [9]. Clearly, the variation of Cp in the range 10–30 K agrees with the low-dimensional character of the system while the peak at 5.3 K confirms the magnetic susceptibility results.

3.2.3. *Magnetic analysis*

An analysis of the magnetic data has been carried out by assuming a model of spin $\frac{1}{2}$ Heisenberg triple chain, which is convenient to describe the above copper(II) compound in the paramagnetic regime. The numerical procedure used, initiated by Bonner and Fisher [10] for spin $\frac{1}{2}$ linear chains and further extended to more exotic systems [11], is based on the diagonalization of the energy matrix by taking into account the geometrical and spin space symmetries of a closed chain. This allows to rule out the drawback encountered with linear finite chain. Then, the thermodynamic properties are computed by the usual procedure [12].

In the case under consideration, five different exchange interactions within the triple chain have been considered in the spin hamiltonian $H = -\sum J_\alpha S_I S_J$, in agreement with structural findings (inset of Fig. 7). Although the distances between copper(II) ions are in the range 3–3.27 Å, no interaction was neglected, because of the dependence of Cu–O–Cu angles and O^{2-} (or OH^-) bridging ligands on the exchange constants. The fitting routine has been performed for a fragment of 12 spin-$\frac{1}{2}$ —a further step with 15 spins was too time consuming—giving a realistic picture of the

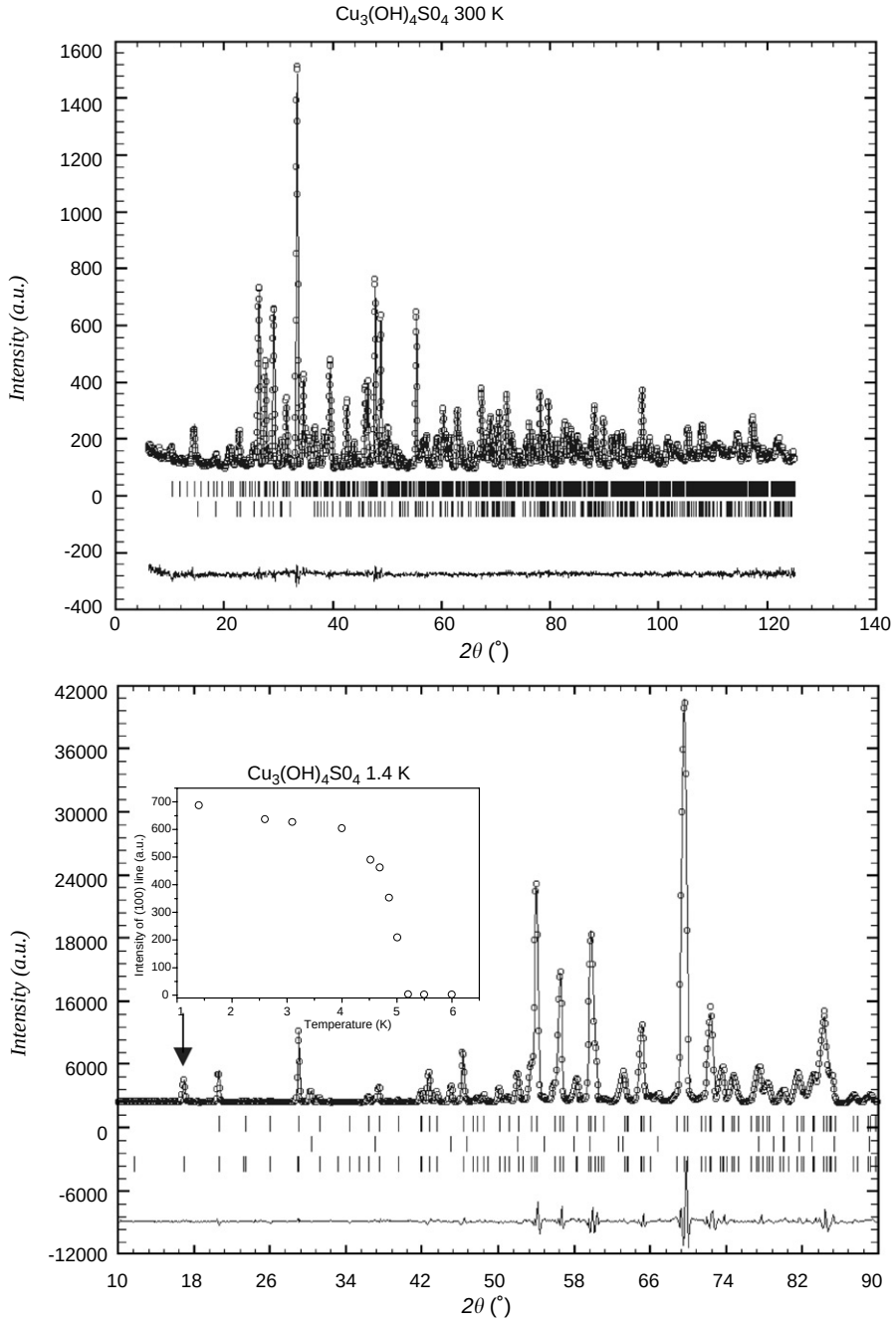

Fig. 5. Upper part: observed (dotted line) and calculated (solid line) profiles of the powder neutron pattern of antlerite obtained on the 3T2 diffractometer at 300 K with position of the Bragg reflections (short vertical lines, first line for antlerite, second line for Na_2SO_4) and difference between observed and calculated profiles. Lower part: Observed (o) and calculated (solid line) profiles of the powder neutron pattern of antlerite obtained on the G4.1 diffractometer at 1.4 K, with just below the difference between observed and calculated profiles. The short vertical lines below the patterns mark the position of all Bragg reflections (nuclear antlerite, nuclear Na_2SO_4 and magnetic lines). The arrow evidences the (1 0 0) magnetic line. Inset: Thermal evolution of the integrated intensity of the (1 0 0) magnetic Bragg peak.

thermodynamics of the infinite system. Using the Landé factor $g = 2.063$ determined from the room temperature χT value, a very good agreement between theory and experiment was obtained for the parameters $J_1 = 2.8$ K, $J_2 = 58.8$ K, $J_3 = 2.6$ K, $J_4 = -9.5$ K and $J_5 = -4.6$ K for the range $8 < T < 300$ K, i.e., for temperatures higher than the 3D transition (Fig. 7). Clearly, the system may appear overparametrized, and so several fits have been performed to test the validity of the results. In fact, the temperature dependence of the χT product is very sensitive to small changes of the exchange constants, and the set of parameters given above seems to be quite

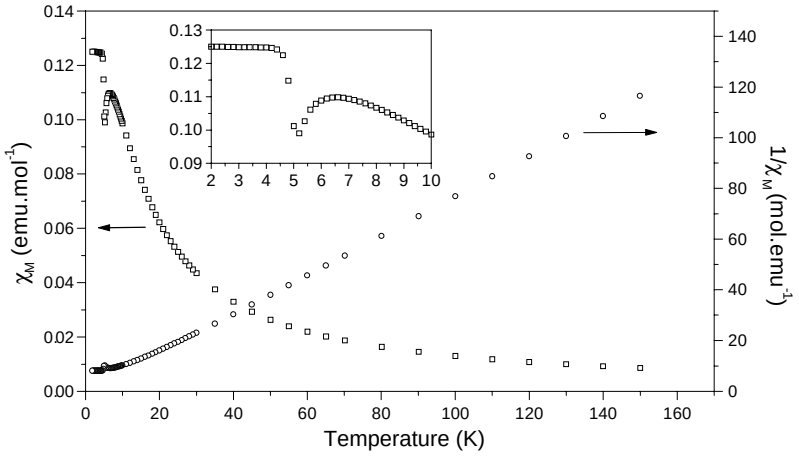

Fig. 6. Magnetic susceptibility and its inverse evolutions versus temperature for antlerite. (Magnetic susceptibility measured under a 100 Oe applied magnetic field). Inset: low-temperature domain of the χ evolution exhibiting the transition.

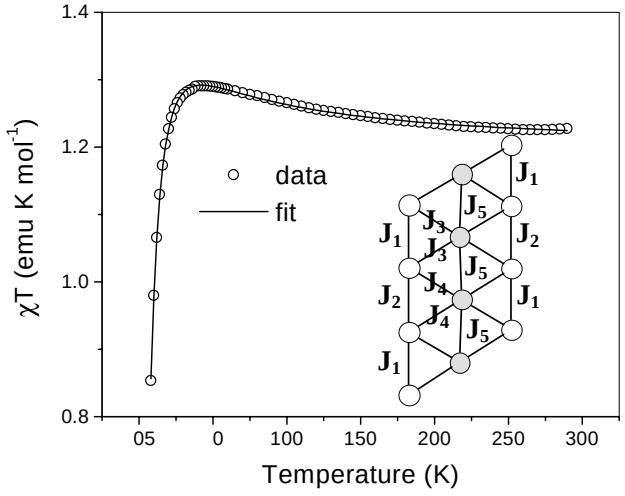

Fig. 7. Experimental and fit data of the evolution of the χT product versus temperature, with a scheme defining the corresponding J coupling constants.

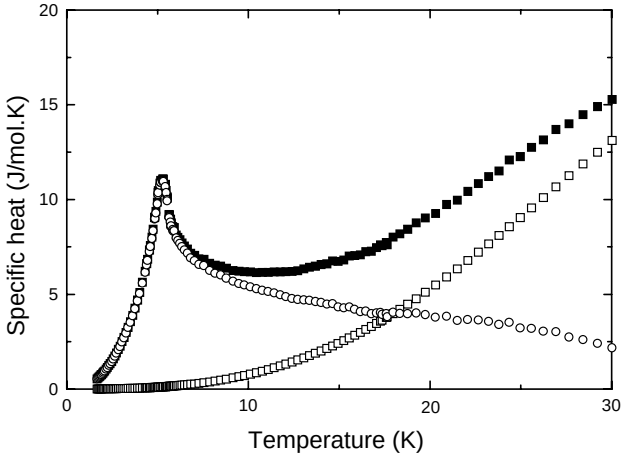

Fig. 8. Specific heat evolution versus temperature: ■, for experimental points; O, for calculated specific heat of magnetic origin; and □, lattice contribution.

realistic (within an error of about 10%), even if the lowest J values are smaller than the temperature range under consideration.

The magnetic structure in the ordered state has been solved from the neutron powder diffraction data collected between 1.4 and 6 K. First, the nuclear structure has been refined starting from the room temperature findings. No magnetic contribution is evidenced down to 5 K, but at lower temperature one new reflection (arrow on Fig. 5) clearly appears for $2\theta = 16.96^\circ$ ($d = 8.2258$ Å), corresponding to the (1 0 0) Bragg peak systematically absent in *Pnma* space group. Its intensity versus temperature is depicted in the inset of Fig. 5. Other very small magnetic contributions are observed, particularly at $2\theta = 41.94^\circ$, 50.63°, 52.53° and 53.43°. The magnetic structure at 1.4 K is in agreement with the results of magnetic susceptibility. It can be viewed as a copper(II) triple chain, consisting of ferromagnetic outer chains (Cu2 atoms), with magnetic moments in the c-axis direction (0.88(5) μ_B) antiparallel to each other (Fig. 9). As regards the central chain (Cu1 atoms), the best fit gives a zero magnetic moment on metal ions, while a spin-$\frac{1}{2}$ is expected for copper(II). The observed and calculated diffraction patterns are shown in Fig. 5.

3.3. Discussion

The structural study reported above does not evidence any significant difference between natural and synthetic antlerites. A 1.7% volume increase, regularly distributed on the three axis directions ($a = 8.289$ Å for 8.244 Å, $b = 6.079$ Å for 6.043 Å and $c = 12.057$ Å for 11.987 Å) in the case of the synthetic compound could be related to the presence of small impurity amounts in the former one. The lack of chemical analysis on the mineral does not allow to identify their nature. Using D_2O and NaOD, it has been possible to prepare antlerite with a

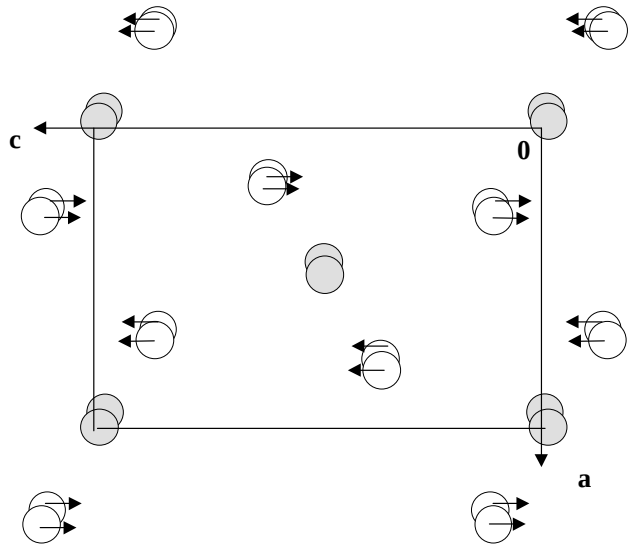

Fig. 9. Projection on the *ac* plane showing the orientations of the magnetic moments.

high D content, around 94%, as evidenced by neutron data refinement.

The infrared spectrum reveals the presence of two bands at 3573 and 3485 cm^{-1} attributed to OH stretching vibrations of OH groups not involved in hydrogen bonding. They can be assigned to (H1 + H2) and H3 according to their relative intensities and to the corresponding occupation numbers of hydrogen atoms, namely 4*c* positions for H1 and H2, 8*d* position for H3. Considering the structure refinement from neutron data, it appears that the O–H/D distances are very similar, 0.955, 0.962 and 0.963 Å for H1, H2 and H3, respectively. Therefore, we have to consider the possible influence of O3 atoms on the O–H stretching vibration by varying its force constant. For the sulfate group, if the distortion from T_d symmetry is rather low, the small observed deviations lower the local symmetry to C_{2v}, as expected from the observation of three bands for ν_3 and ν_4 as well as from the presence of the ν_1 vibration band.

The proposed magnetic structure in the ordered state agrees well with the results of magnetic susceptibility. Each triple chain exhibits an antiferromagnetic ground state, but it appears that interactions of opposite signs concur to the overall behavior. Thus, the magnetic moments of the outer chains (Cu2) order ferromagnetically (J_1 and J_2 interactions) and are aligned antiparallel to each other, while the moments of the central chain (Cu1) are antiferromagnetically coupled. Furthermore, these individual chains are connected through the J_3 and J_4 exchange couplings giving rise to a strongly correlated ribbon. Note that the large ferromagnetic interaction J_1, which favors a dimerized structure in the Cu2 chains, explains the variation of the χT product in the range 40–300 K. At lower temperature, the other (positive and negative) interactions promote a spin singlet for the triple chain, and accordingly χT decreases to zero. Finally, both susceptibility and specific heat measurements reveal that at about 5 K a transition occurs which stabilizes a long-range 3D order between triple chains. The mechanism involved may be a classical quantum interaction through (SO_4) units or, more likely, a dipolar coupling between ribbons which would be supported by the presence of outer ferromagnetic chains [13].

The zero magnetic moment obtained for Cu1 from the neutron diffraction experiments is at first questionable. In fact, this may be explained by some misorientation of the magnetic moments due to the competition between different interactions and a negligible local anisotropy. Other magnetic structure refinements have been considered, involving antiferromagnetic order inside the Cu1 central chains, but all lead to insignificant values of the moment, always much lower than standard deviations. Such behavior, so-called "idle-spin" behavior, was already evidenced for other compounds [14–17].

It is known that the exchange coupling in copper(II) compounds is closely related to the bridging angle Cu–O–Cu. Thus, it has been demonstrated [18] for a series of di-μ-hydroxo-bridged copper(II) compounds that positive J values are observed for a bridge angle ϕ lower than 97.5°, whereas higher ϕ values favor a negative exchange constant.

For the title compound, the pertinent exchange pathways within copper(II) ribbons call for the following remarks:

- Cu1 ions are bonded to each other through two hydroxo (OH3) with a bridging angle $\phi = 99.6°$, favoring an antiferromagnetic coupling (J_5).
- Cu2 ions are bonded to each other through an hydroxo and an oxygen atom. Along the Cu2 chain, we have alternatively (O1 + OH1) and (O2 + OH2) bridging units. The ϕ angle values are less than 90° for bridging oxygen atoms and larger than 97.5° for both hydroxo bridges. The ferromagnetic interactions J_1 and J_2 entail that the dominant pathways are through oxygen atoms, even if the Cu2–O bond lengths (2.43 and 2.36 Å) are significantly larger than the Cu2–OH ones (1.94 and 1.93 Å),
- Cu1 and Cu2 chains are alternatively bonded through hydroxo and oxygen bridges. As above, the presence of two hydroxo bridges implies an antiferromagnetic coupling (J_4) whereas mixed oxygen and hydroxo bridges favor a ferromagnetic coupling (J_3)

4. Conclusion

Antlerite, $Cu_3(OH)_4SO_4$, obtained by hydrothermal synthesis, has been characterized by its structural and magnetic properties. Triple chains of edge sharing

copper octahedra running in the *b*-axis direction are connected to each other through sulfate tetrahedra. Both neutron diffraction study and magnetic susceptibility fit agree with a model involving the same interactions between copper ions. The results have also been related to the Cu–O–Cu angle values. It is to be noted that such compound may be viewed as a new class of low-dimensional system, in between 1D and 2D systems, which may exhibit unusual quantum effects. Other members of the series are investigated, as for instance brochantite, $Cu_4(OH)_6SO_4$.

References

[1] M. Richard-Plouet, S. Vilminot, J. Mater. Chem. 8 (1998) 131–137.
[2] M. Richard-Plouet, S. Vilminot, Solid State Sci 1 (1999) 381–393.
[3] M. Guillot, M. Richard-Plouet, S. Vilminot, J. Mater. Chem. 12 (2002) 851–857 (doi:10.1039/b110101c)..
[4] C.K. Majumdar, D.K. Gosh, J. Math. Phys. 10 (1969) 1388.
[5] F.C. Hawthorne, L.A. Groat, R.K. Eby, Can. Mineral. 27 (1989) 205–209.
[6] J. Rodriguez-Carvajal, FULLPROF: Rietveld, Profile Matching and Integrated Intensity Refinement of X-ray and/or Neutron Data, Version 3.3 Léon-Brillouin Laboratory, C. E. A.-Saclay, France, 1997.
[7] K. Nakamoto, Infrared and Raman Spectra of Inorganic and Coordination Compounds, Wiley-Interscience, New York, 1986, p. 248.
[8] J. Stolz, T. Armbruster, N. Jb. Miner. Mh. 6 (1998) 278–288; P. C. Burns, Mineral. Mag 62 (1998) 461–469.
[9] R.L. Carlin, Magnetochemistry, Springer, Berlin, Heidelberg, 1986, p. 165.
[10] J.C. Bonner, M.E. Fisher, Phys. Rev. A 135 (1964) 640.
[11] R. Georges, J.J. Borras, E. Coronado, J. Curely, M. Drillon, Magnetism: molecules to materials, Models and Experiments, In: J. Miller, M. Drillon, (Eds.), Wiley VCH, Weinheim, 2001, pp. 1–47.
[12] M. Drillon, E. Coronado, R. Georges, J.C. Gianduzzo, J. Curely, Phys. Rev. B 40 (1989) 10992–10998.
[13] S. Ostrovsky, W. Haase, M. Drillon, P. Panissod, Phys. Rev. B 64 (2001) 134418/1–134418/17.
[14] G. Courbion, R. De Pape, J. Teillet, F. Varret, J. Pannetier, J. Magn. Magn. Mater. 42 (1984) 217–232.
[15] M. Guillot, A. Marchand, M. Leblanc, G. Ferey, J. Phys. C 20 (1987) 2405–2414.
[16] M.A.G. Aranda, J.P. Attfield, E. Batchelor, G.P. Shields, S. Bruque, M. Gabas, Inorg. Chem. 37 (1998) 1329–1335.
[17] M. Guillot, M. El-Ghozzi, D. Avignant, G. Andre, F. Bouree, A. Cousson, J. Appl. Phys. 191 (2002) 8519–8521.
[18] V.H. Crawford, H. Wayne Richardson, J.R. Wasson, D.J. Hodgson, W.E. Hatfield, Inorg. Chem. 15 (1976) 2107–2110.